FLOW PROFILES OF POWER LAW FLUIDS IN SCRAPED SURFACE HEAT EXCHANGER GEOMETRY USING MRI

WEI WANG, JEFFREY H. WALTON[1] and KATHRYN L. McCARTHY[2]

Department of Biological and Agricultural Engineering
NMR Facility[1]
University of California, Davis
Davis, CA 95616

Accepted for Publication September 11, 1998

ABSTRACT

Scraped surface heat exchangers (SSHE) are prevalent in the food industry to heat/cool viscous fluids and to provide enhanced mixing. This work focused on developing and verifying a theoretical model to characterize the flow patterns in two-dimensional angular flow in an SSHE geometry under isothermal conditions. Experimentally, the model was verified by a noninvasive magnetic resonance imaging (MRI) technique. Good agreement was achieved between the theoretical model and experimental data for a polyalkylene glycol, which behaved as a Newtonian fluid ($n = 1$), and a 1% CMC solution, a power law fluid with $n = 0.77$. However, the experimental flow profile tomato puree was characterized by apparent wall slip. The best fit, with respect to the power law model, was a flow behavior index of 0.11. This study provides the framework to quantify the effects of heat transfer on flow profiles in this geometry and the effectiveness of mixing.

INTRODUCTION

Scraped surface heat exchangers (SSHE) are essential for the continuous processing of high viscosity fluids and fluids containing particles in the food and chemical industries. In previous studies, characterization of the SSHE was focused on residence time distribution, heat transfer coefficient and power requirement using similarity methods, dimensional analysis or theoretical considerations in terms of shaft rotation speeds, rheological properties of fluids, annulus gap widths and axial flow rates. Although this information is useful in terms of controlling an individual SSHE, it is difficult to generalize the results to other scraped surface heat exchangers.

[2] To whom correspondence should be addressed. Tel. 530-752-1487; Fax: 530-752-4759

Journal of Food Process Engineering **22** (1999) 11–27. *All Rights Reserved.*

This study focuses on the flow profile in a SSHE, since the flow profile controls mixing and thermal-time effects in the exchanger. The ability to quantify these phenomena is essential in order to model the heat transfer mechanism and optimize heat exchange. The two primary flow directions of the fluid are flow in the angular direction due to rotation and flow in the axial direction due to the imposed pressure gradient. The velocity components of the two flows form a helical path for the product through the SSHE. A complete mixing in the angular direction is desired to maximize the efficiency of heat transfer and ensure uniform thermal treatment. At the same time, the mixing in the axial direction should be minimized due to the fact that the axial mixing increases the residence time distribution of the product in the SSHE (Abichandani *et al.* 1987; Härröd 1986).

An early study by Trommelen and Beek (1971) to evaluate the velocity profile of a Newtonian fluid in an SSHE was performed with a photographic method. To obtain the velocity profile, the outer cylinder of an SSHE was kept stationary while the dye was injected. Then the outer cylinder was rotated manually through an angle of approximately 20 degrees. A photograph was taken after each rotation and the displacement of the dye was determined. The information was plotted as velocity versus radial position. The researchers compared the velocity profiles for different types of blades. For cutaway blades, the velocity profile was similar to Couette flow. The velocity profile for closed blades was similar to the pressure-driven flow between two parallel plates with one plate moving. However, due to experimental errors, the difference between the experimental velocity profile and theoretical analysis based on the Navier-Stokes equation was large.

More recent flow visualization studies have incorporated the use of magnetic resonance imaging (MRI). A review by Caprihan and Fukushima (1990) describes the most common methods used for NMR flow imaging. Arola *et al.* (1997) and McCarthy (1994) provide references for work published since then, the most common geometries for NMR flow visualization being pipe flow and concentric cylinders. The angular velocity of fluid in an SSHE geometry was first studied using NMR flow visualization by Corbett *et al.* (1995). The experimental MRI velocity profiles of polyalkylene glycol (a Newtonian fluid) showed excellent agreement with the analytical solution from the Navier-Stokes equation.

Since many food products exhibit non-Newtonian behavior, this work extends the work performed by Corbett *et al.* (1995) to power law fluids. The objective of this research was to develop a model to characterize the angular velocity profiles of power law fluids in the scraped surface heat exchanger and to verify the model using an NMR flow visualization technique.

THEORETICAL MODEL

The theoretical model is based on the conservation of momentum for an isothermal incompressible fluid under steady state flow conditions in the annular region of the scraped surface heat exchanger. A blade is attached to the inner cylinder as shown in Fig. 1. The inner cylinder/blade is rotated at an angular rotation speed of ω and the blade sweeps all fluid in the annulus. Therefore, the blade is characterized as a closed type in this model with an inner cylinder radius designated as R_i and the outer cylinder radius designated as R_0. The ratio of the inner cylinder and the outer cylinder radii is κ (Fig. 2).

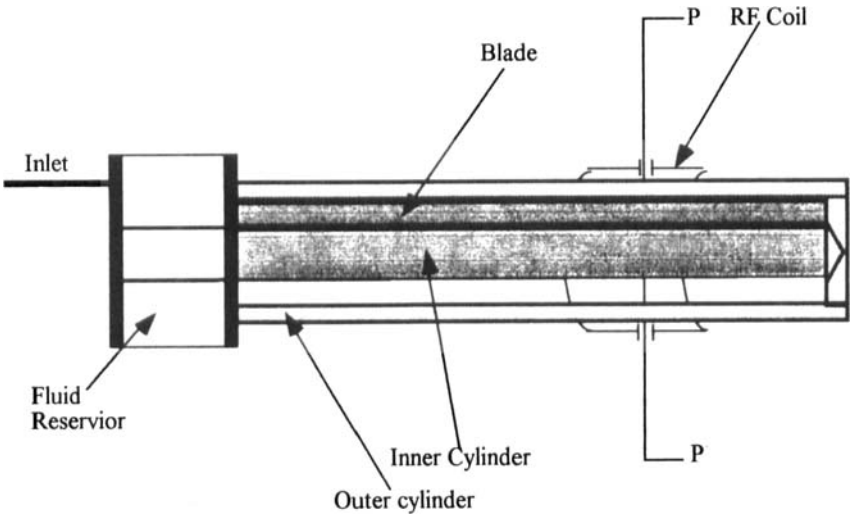

FIG. 1. SCHEMATIC OF THE SCRAPED SURFACE HEAT EXCHANGER GEOMETRY
The imaging plane is the cross section at the position designated as P–P.

The flow pattern of power law fluids is evaluated in the region away from the flight where the angular velocity is only a function of radius r, $v_\theta = f(r)$. Further assumptions for the model include: (1) laminar flow; (2) no-slip conditions at the solid surfaces; and (3) no radial or axial velocity components.

Based on the above assumptions, only the v_θ component of the velocity vector is considered in the analysis. For these conditions, the stress equation of motion in θ-direction is reduced to:

$$\frac{1}{r}\frac{\partial P}{\partial \theta} = \frac{1}{r^2}\frac{\partial}{\partial r}\left(r^2 \tau_{r\theta}\right) \tag{1}$$

where $\partial P/\partial\theta$ is the pressure gradient in θ-direction. The relationship of shear stress $\tau_{r\theta}$ to rate of deformation tensor (Δ) and apparent viscosity (η) for a power law fluid is simplified to an expression in terms of the gradient of the angular velocity v_θ (Bird *et al.* 1960):

$$\tau_{r\theta}=\eta\Delta=K\left|\sqrt{\frac{1}{2}\Delta:\Delta}\right|^{n-1}\Delta=K\left|r\frac{\partial}{\partial r}\left(\frac{v_\theta}{r}\right)\right|^{n-1}\left[r\frac{\partial}{\partial r}\left(\frac{v_\theta}{r}\right)\right] \tag{2}$$

where K is the consistency index and n is the flow behavior index. To perform the analytical integration of Eq. (1) to obtain the velocity profile, the flow behavior index must be specified and $1/n$ must be an integer (CRC 1991). Although the calculation procedures below are for a Newtonian fluid (n = 1), the same approach was used for n = 1/2, 1/3, 1/4, 1/5, 1/7 and 1/9 (Wang 1997).

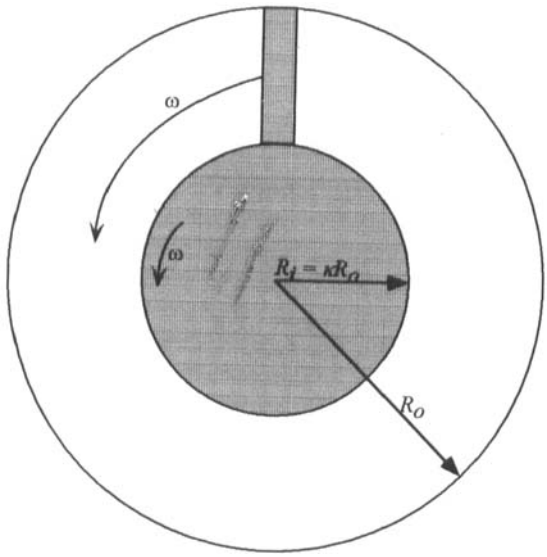

FIG. 2. CROSS SECTION OF THE SCRAPED SURFACE HEAT EXCHANGER GEOMETRY

The shaded regions are the inner cylinder and the blade, rotating at angular velocity ω.

In order to integrate Eq. (1), a new radial parameter R^* is introduced to identify the radial location at which the velocity gradient is zero. From $R_i < r < R^*$, the velocity gradient, $r\frac{\partial}{\partial r}\left(\frac{v_\theta}{r}\right)$ is positive. From $R^* < r < R_0$, the velocity gradient is negative. Because the velocity profile is not symmetric, these

regions are considered separately. Although this approach is not necessary with a Newtonian fluid, it is necessary when $1/n$ is an integer other than 1 (*e.g.*, $n < 1$).

For Region (1) where $R_i < r < R^*$ and the velocity gradient $r\frac{\partial}{\partial r}\left(\frac{v_\theta}{r}\right) > 0$, the momentum equation is:

$$\frac{1}{r^2}\frac{\partial}{\partial r}\left\{r^2 K\left[r\frac{\partial}{\partial r}\left(\frac{v_\theta}{r}\right)\right]^n\right\} = \frac{1}{r}\frac{\partial P}{\partial \theta} \tag{3}$$

To provide a more general solution, Eq. (3) is expressed in a dimensionless form; the dimensionless parameters are defined as: velocity, $\hat{v}_\theta = \frac{v_\theta}{V_{ave}} = \frac{v_\theta}{\frac{R_i + R_o}{2}\omega}$ radial position, $\hat{r} = \frac{r}{R_o}$; and pressure gradient, $\frac{\partial \hat{P}}{\partial \hat{\theta}} = \frac{1}{2K\omega^n}\frac{\partial P}{\partial \theta}$.

For a flow behavior index of 1, Eq. (3) was converted to a dimensionless expression and integrated twice. Upon evaluation the boundary conditions $\hat{v}_\theta^+ = 2\kappa/(\kappa+1)$ at $\hat{r} = \kappa$ and $\hat{r}\frac{\partial}{\partial \hat{r}}\left(\frac{\hat{v}_\theta}{\hat{r}}\right) = 0$ at $\hat{r} = \hat{R}^*$, the velocity profile with positive shear rate, $\hat{v}_\theta^+$, is:

$$\hat{v}_\theta^+ = \frac{\partial \hat{P}}{\partial \hat{\theta}}\left[\hat{r}\ln\frac{\hat{r}}{\kappa} + \frac{\hat{R}^{*2}}{2}\left(\frac{1}{\hat{r}} - \frac{\hat{r}}{\kappa^2}\right)\right] + \frac{2\hat{r}}{1+\kappa} \tag{4}$$

In Region (2) where $R^* < r < R_0$ and $r\frac{\partial}{\partial r}\left(\frac{v_\theta}{r}\right) < 0$, the momentum equation is:

$$\frac{1}{r^2}\frac{\partial}{\partial r}\left\{-r^2 K\left[-r\frac{\partial}{\partial r}\left(\frac{v_\theta}{r}\right)\right]^n\right\} = \frac{1}{r}\frac{\partial P}{\partial \theta} \tag{5}$$

Integrating and implementing the boundary conditions $\hat{v}_\theta = 0$ at $\hat{r} = 1$ and

$\hat{r}\dfrac{\partial}{\partial \hat{r}}\left(\dfrac{\hat{v}_\theta}{\hat{r}}\right) = 0$ at $\hat{r} = \hat{R}^*$ yields the velocity profile with the negative velocity

$$\hat{v}_\theta^- = \frac{\partial \hat{P}}{\partial \hat{\theta}}\left[\hat{r} \ln \hat{r} + \frac{\hat{R}^{*2}}{2}\left(\frac{1}{\hat{r}} - \hat{r}\right)\right] \tag{6}$$

In Eq. (4) and (6), $\partial \hat{P}/\partial \hat{\theta}$ and $\hat{R}^*$ are unknown and two more conditions are required to solve for the velocity profiles. The first condition requires that the values of $\hat{v}_\theta^+$ and $\hat{v}_\theta^-$ be equal at $\hat{r}=\hat{R}^*$. The second condition is that the net angular volumetric flow rate is the volume of fluid swept by the blade during a unit time by the closed blade. By applying the first condition and combining Eq. (4) and (6), the angular pressure gradient is:

$$\frac{\partial \hat{P}}{\partial \hat{\theta}} = \frac{\dfrac{4}{(1+\kappa)}}{\left[2 \ln \kappa + \hat{R}^{*2}\left(\dfrac{1}{\kappa^2} - 1\right)\right]} \tag{7}$$

Using the second condition, the dimensionless volumetric flow rate per unit length is expressed in terms of $\hat{v}_\theta^+$ and $\hat{v}_\theta^-$ as:

$$\hat{Q} = 1 - \kappa = \int_\kappa^{\hat{R}^*} \hat{v}_\theta^+ d\hat{r} + \int_{\hat{R}^*}^1 \hat{v}_\theta^- d\hat{r} \tag{8}$$

Evaluating this expression for $\partial \hat{P}/\partial \hat{\theta}$ and $\hat{R}^*$ yields:

$$\frac{\partial \hat{P}}{\partial \hat{\theta}} = \frac{4(1-\kappa)}{[(1+\hat{R}^{*2})(\kappa^2-1) - 2 \ln \kappa(\kappa^2+\hat{R}^{*2})]} \tag{9}$$

The values of $\partial \hat{P}/\partial \hat{\theta}$ and $\hat{R}^*$ can be solved either graphically or numerically by substituting $\hat{r}$ for $\hat{R}^*$ in Eq. (7) and (9) in the range of $\kappa \leq \hat{r} \leq 1$. The intersection of the two curves is the solution for $\partial \hat{P}/\partial \hat{\theta}$ and $\hat{R}^*$; values of these parameters for the experimental geometry are given in Table 2 for integer values of $1/n$. The values of $\partial \hat{P}/\partial \hat{\theta}$ and $\hat{R}^*$ are incorporated into the velocity profile expressions, $\hat{v}_\theta^+$ and $\hat{v}_\theta^-$. In the cases when $1/n$ is odd (*e.g.*, $n = 1, 1/3, 1/5$), the velocity profiles of $\hat{v}_\theta^+$ and $\hat{v}_\theta^-$ are essentially the same curves. However,

when $1/n$ is even, (*e.g.*, n = ½, ¼), $\hat{v}_\theta^+$ and $\hat{v}_\theta^-$ are not the same curves. Figures 3 and 4 illustrate the velocity profiles $\hat{v}_\theta^+$ and $\hat{v}_\theta^-$ for the flow behavior indices of 1 and ½, respectively.

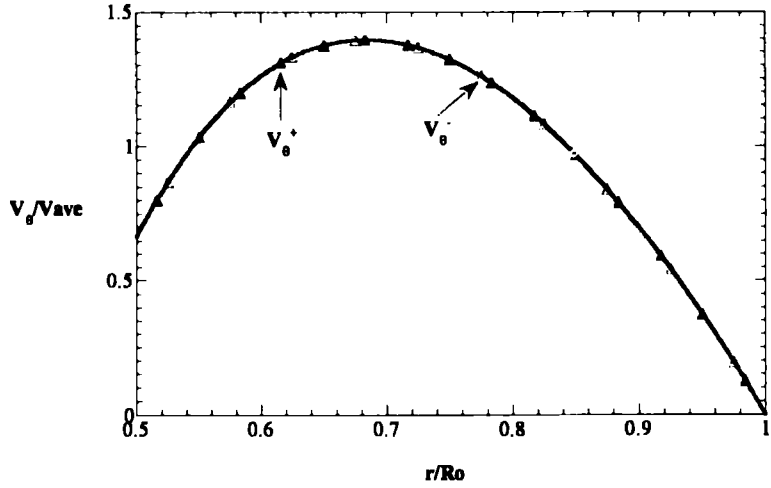

FIG. 3. DIMENSIONLESS VELOCITY PROFILES FOR A NEWTONIAN FLUID, WITH THE VELOCITY PROFILE FOR THE POSITIVE SHEAR RATE, v_θ^+ (▲) AND THE VELOCITY PROFILE FOR THE NEGATIVE SHEAR RATE, v_θ^- (Δ)

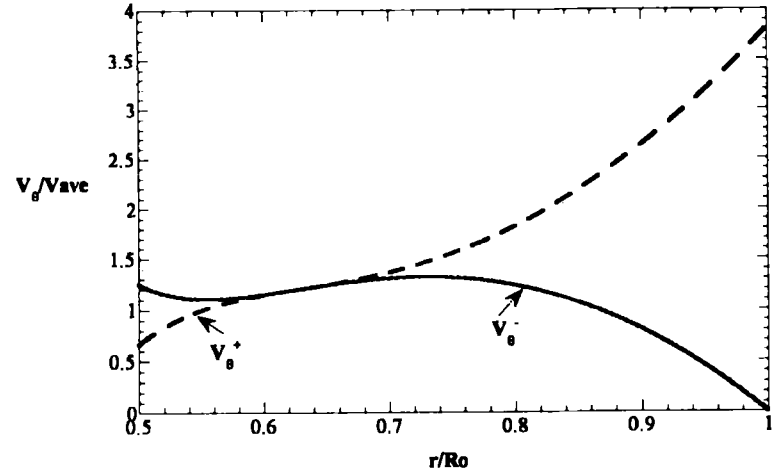

FIG. 4. DIMENSIONLESS VELOCITY PROFILES FOR A POWER LAW FLUID (n = ½), WITH THE VELOCITY PROFILE FOR THE POSITIVE SHEAR RATE, v_θ^+ (--) AND THE VELOCITY PROFILE FOR THE NEGATIVE SHEAR RATE, v_θ^- (—).

Numerical Simulation

A finite element numerical technique was also used to solve the conservation of momentum equation in the SSHE geometry. This method is a widely accepted numerical procedure for solving differential equations in the areas of structural analysis, heat transfer and fluid flow (Reddy 1984; Segerlind 1984). As a numerical technique, it has two advantages in this geometry over the analytical solution: the flow behavior indices are not limited to integer values of $1/n$ and the angular velocity is determined as a function of both angular and radial position.

The commercially available software, Fluid Dynamics Analysis Package (FIDAP) (Fluent Inc., Evanston, IL) was used for the numerical simulation. A two-dimensional analysis was performed using the same dimensionless parameters and boundary conditions as the analytical solution above. Each element was quadrilateral-shaped and composed of 4 nodes. The successive substitution solution algorithm, in which all the equations were fully coupled and solved simultaneously, was used. The simulation was run for the Newtonian and the power law fluids, with the fluid behavior indices of 1, 1/2, 1/3, 1/4, 1/5, 1/7 and 1/9. A sensitivity analysis was done to ensure convergence (Wang 1997). The velocity profile was extracted across the radial direction opposite the blade to compare with the analytical solution. Velocity profiles for selected values of the flow behavior index are shown in Fig. 5; the agreement between the two solution techniques is excellent.

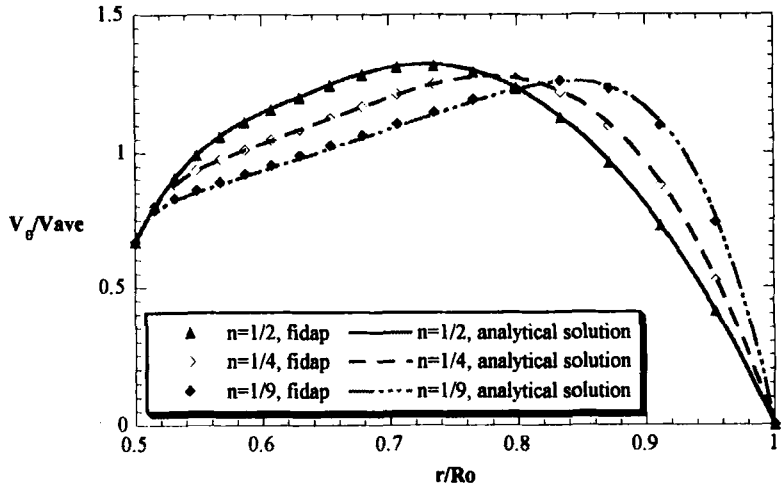

FIG. 5. COMPARISONS OF VELOCITY PROFILES FROM ANALYTICAL SOLUTION AND NUMERICAL SIMULATION FOR FLOW BEHAVIOR INDICES OF 1/2, 1/4, AND 1/9

MATERIAL AND METHODS

MRI Experiments

The analytical and numerical solutions of the momentum equation were experimentally verified by an MRI technique. Due to imaging constraints, the scraped surface heat exchanger geometry used in the MRI experiments was nonmagnetic and nonmetal (Fig. 1). The geometry consisted of a 1.91 cm ID × 30 cm cylinder with a straight 0.318 cm × 0.953 cm blade fabricated of polyethyleneterephthalate (PET). This cylinder fit within an acrylic outer cylinder with a 3.81 cm ID. The blade swept the entire volume of the annular region; therefore, the SSHE geometry was considered a closed type. The inner cylinder/blade rotated with an angular frequency ω as shown in Fig. 2. There was no flow in the axial direction during any of these experiments.

Three fluids, ranging from Newtonian to highly non-Newtonian, were used in the experiment to evaluate the velocity profiles in the angular direction. They were polyalkylene glycol, a water soluble oil (UCON, Union Carbide Corp., Danbury, CT), 1% carboxymethyl cellulose aqueous solution (CMC, Sigma Chemical Co., St. Louis, MO), and tomato puree at 9° Brix (Pomi Strained tomatoes, Parmalat U.S.A. Inc., Hasbrouck Hts., NJ). Rheology measurements was performed with a Haake RV20 (Gebrüder Haake GmbH, Karlsruhe, Germany) over a range of shear rate of 0-10 s^{-1}, which corresponded to the MRI experimental studies. The three fluids were modeled as power law fluids, with the Newtonian fluid having a flow behavior index of one. The rheological properties, as well as the angular Reynolds number, are listed in Table 1. The sample was loaded into the SSHE and filled the annular region and reservoir. The apparatus was placed into the magnet and the inner cylinder/blade was attached to the drive motor shaft.

TABLE 1.
RHEOLOGICAL MEASUREMENTS PERFORMED WITH A HAAKE RV20, OVER A SHEAR RATE RANGE APPROPRIATE FOR THE EXPERIMENTAL APPARATUS

Test Fluids	Consistency Index ($Pa \cdot s^n$)	Flow Behavior Index, n	Shear Rate (1/s)	$Re_{angular}$
UCON Oil	5.4	1.0	-	0.127
1% CMC	3.5	0.77	0 - 10	0.0752
Tomato Puree	9.2	0.28	0 - 10	0.0602

The NMR images were obtained with a 0.6 Tesla General Electric CSI-2 spectrometer (Fremont, CA), upgraded with a Tecmag Libra Pulse Programmer/Data Acquisition System and MacNMR™ (Tecmag, Inc., Houston, TX) installed on a Macintosh PowerMac model 7100/66 computer (Apple Computer, Inc., Cupertino, CA). A "birdcage" coil with an inner diameter of 7.61 cm and a length of 11.3 cm was fitted outside the outer cylinder of the SSHE acting as a r.f. pulse transmitter and as a signal receiver. The center of the coil was located at the axial position of 20.5 cm relative to the fluid reservoir.

The MRI flow visualization technique was a "time-of-flight" method. This type of technique magnetically nulls or "tags" a selected volume of fluid noninvasively (McCarthy 1994). Initially, this tagged volume is a horizontal stripe across the cross sectional plane of the apparatus. After a specified time interval, scans are taken to construct an image to observe the displacement of the nulled fluid. These image files were transferred into a Matlab-equipped computer (MathWorks, Inc., Natick, MA) for image processing.

The local velocity as a function of radial position was determined by the quotient of the displacement of the nulled fluid and the time interval. Specifically, the processing of each image included thresholding, normalizing the signal intensity from 0 to 255, and identifying the spatial location of the tagged fluid. The spatial position of the tagged material during flow was then compared to the original position of tagged material ($t=0$). Using the flow time and displacement of the tagged band, the velocity was determined. The Cartesian velocity and spatial position was then converted to cylindrical coordinates. For ease of comparison to the theoretical model, the velocity was made dimensionless using the average velocity and the radial position was made dimensionless by the outer cylinder radius.

RESULTS AND DISCUSSIONS

Blade Type

The limiting cases for the flow profiles in SSHE geometry are illustrated in Fig. 6. The theoretical curves represent a closed blade and an open blade. The maximum pressure gradient is created with the closed type blade (designated in the figure as SSHE). The velocity profile is asymmetric and the maximum velocity is greater than the velocity of the rotating cylinder/blade. For a Newtonian fluid (shown), the maximum velocity is at approximately one-third the distance between the inner and outer cylinder.

In contrast, the open type blade prevents the development of a pressure gradient in the annular direction. In the limit, the flow profile is similar to Couette flow shown in Fig. 6. The maximum velocity under these conditions is at the rotating surface. As evidenced by the area under the curves in Fig. 6, the

volumetric flow rate in the angular direction of the SSHE profile is significantly greater than that of Couette geometry. Therefore, although the helical flow pattern that was described by Härröd (1986) may be adequate to characterize an open blade SSHE, the pressure gradient in the angular direction of the closed type blade will influence both mixing and heat exchange mechanisms and should be taken into account in flow models for this type blade.

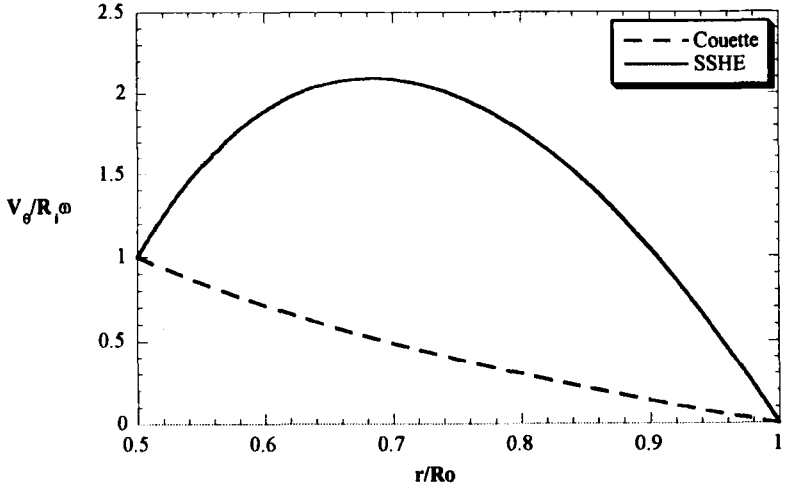

FIG. 6. COMPARISONS OF VELOCITY PROFILES FOR THE LIMITING CASES OF FLOW IN AN SSHE GEOMETRY: OPEN TYPE (COUETTE FLOW) AND CLOSED TYPE

Flow Behavior Index

Figure 5 illustrates the trends in the velocity profile as the flow behavior index decreases. In general, the velocity profile flattens. The pressure gradient $\partial\hat{P}/\partial\hat{\theta}$ and value of $\hat{R}*$ for these curves are given in Table 2. As with pipe flow, the pressure driving force decreases as the flow behavior index decreases.

In contrast to the pressure gradient, the value of $\hat{R}*$ is relatively insensitive to the flow behavior index. In other words, the position of zero shear rate remains at a dimensionless radial position of approximately 0.63. However, the maximum velocity decreases as the flow behavior index decreases, similar to the trend in pipe flow. But unlike pipe flow, the radial position of maximum velocity shifts toward the outer cylinder.

TABLE 2.
DIMENSIONLESS PRESSURE GRADIENT AND DIMENSIONLESS RADIAL POSITION R* AS A FUNCTION OF FLOW BEHAVIOR

Integer values of 1/n	Flow Behavior Index, n	Dimensionless Pressure Gradient	Dimensionless Radial Position
1	1	-13.112	0.628
2	1/2	-5.173	0.626
3	1/3	-3.737	0.626
4	1/4	-3.154	0.626
5	1/5	-2.838	0.625
7	1/7	-2.503	0.626
9	1/9	-2.323	0.626

The trends that are predicted by the theoretical analysis are verified experimentally with the MR imaging. The image and the resulting experimental velocity profile of the Newtonian fluid, UCON oil, are shown in Fig. 7 with the analytical solution. The graph was plotted as dimensionless velocity versus dimensionless radial position. The y-axis, the angular velocity, was made dimensionless using the average velocity in θ-direction. The x-axis, the radial position, was made dimensionless using the outer cylinder radius. The experimental data were compared with the analytical solution of the model for the Newtonian fluid. The correlation of coefficient, R^2, between the experimental data and the analytical solution was 0.9903, exhibiting excellent agreement.

Figure 8 illustrates the image and the resulting experimental velocity profile of the 1% aqueous CMC solution, with a flow behavior index of 0.77. Again, the graph was plotted as dimensionless velocity versus dimensionless radial position. The correlation of coefficient between the experimental data and the numerical solution for $n=0.77$ solution was 0.9975, also exhibiting excellent agreement.

The third fluid was tomato puree (Fig. 9). From Table 1, the flow behavior index of tomato puree was 0.28. Unlike the fluids in Fig. 7 and 8, the velocity profile of the tomato puree was fit to a flow behavior index. Flow behavior indices of 1/4 and 1/9 are shown on Fig. 9, the best fit of the MR experimental data being $n = 1/9$ ($R^2=0.82$). In contrast to the polyalkylene glycol and the 1% CMC solution, the tomato puree was a suspension. To minimize the

possibility of serum separation during the experiment, the image size was reduced from 256 by 128 to 256 by 64. The shorter imaging time minimized the migration of particles at the expense of resolution. Data were much more scattered than in the other sets of experiments and indicate the possibility of apparent wall slip at the outer cylinder ($r/R_o = 1.0$). Although, the scraped surface heat exchanger geometry is designed to promote mixing, the steep velocity gradient at low values of n enhances particle migration and results in serum separation at that surface.

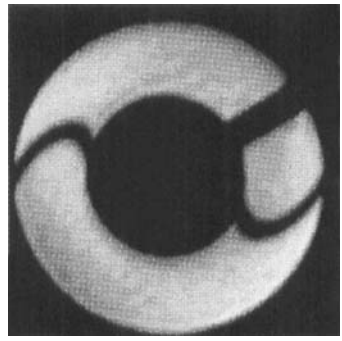

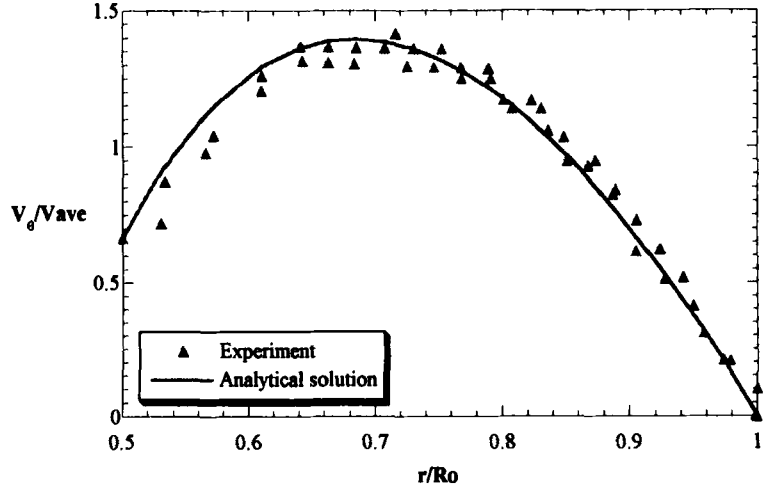

FIG. 7. MR IMAGE AND DIMENSIONLESS VELOCITY PROFILE FOR POLYALKYLENE GLYCOL ($n=1$) IN TWO-DIMENSIONAL FLOW

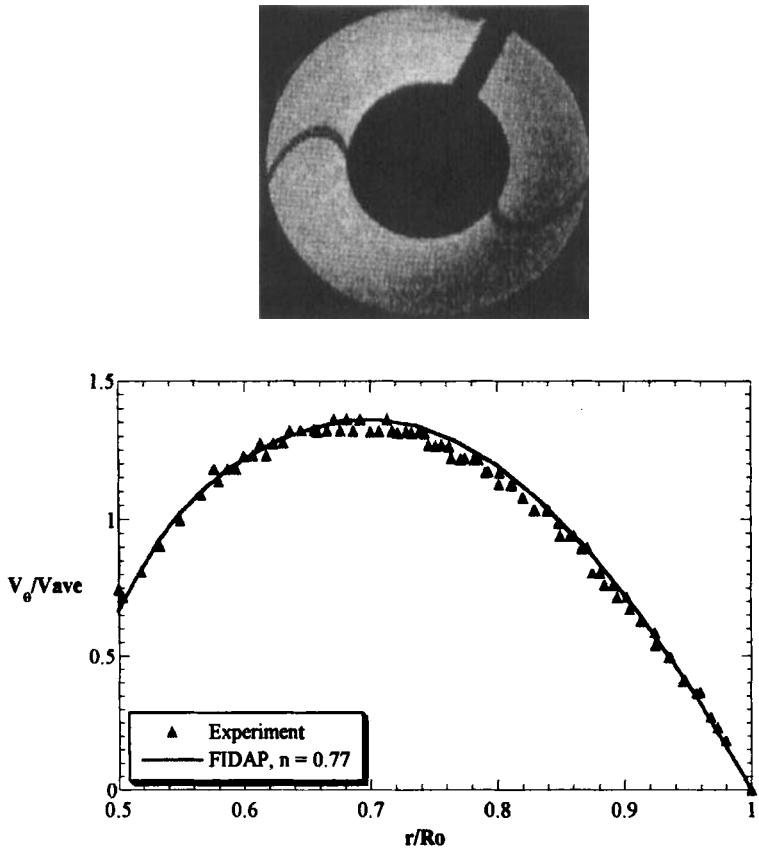

FIG. 8. MR IMAGE AND DIMENSIONLESS VELOCITY PROFILE FOR 1% CMC SOLUTION (n = 0.77) IN TWO-DIMENSIONAL FLOW

CONCLUSIONS

As flow patterns are important in understanding the mixing and heat transfer mechanisms in the scraped surface heat exchangers, this research developed and verified the mathematical model for power law fluids in the closed blade type SSHE. Specifically, the angular velocity profile in the region away from the blade was evaluated theoretically and numerically and compared with MR experimental results. The agreement was excellent for the homogeneous power law fluids. The evidence of apparent wall slip and flattened velocity profile of the tomato puree is a significant step toward the evaluation of mixing and heat transfer of foods processed commercially by SSHEs.

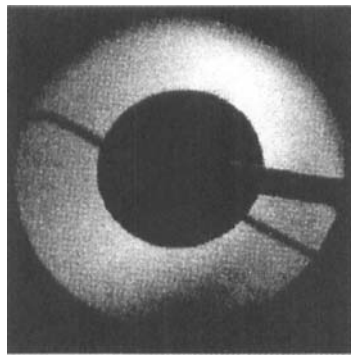

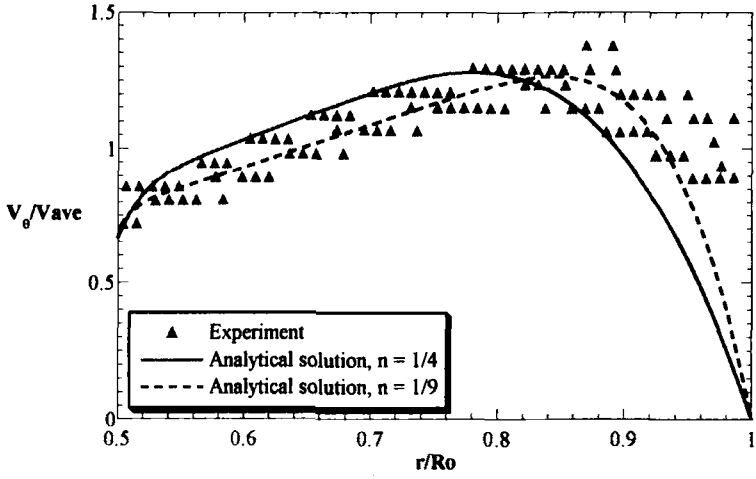

FIG. 9. MR IMAGE AND DIMENSIONLESS VELOCITY PROFILE FOR TOMATO PUREE (n = 0.28) IN TWO-DIMENSIONAL FLOW

ACKNOWLEDGMENTS

Funding for this research was provided by the National Science Foundation (BCS-9057676).

NOTATION

K consistency index, $Pa \cdot s^n$
n flow behavior index

P	pressure, Pa
Q	angular volumetric flow rate, $Q = L\omega(R_0^2-R_i^2)/2$, m^3/s
$\hat{Q}$	dimensionless angular volumetric flow rate in unit length, $(\kappa^{-2}-1)/2$
$Re_{angular}$	Reynolds number in angular direction, $\omega D_0^2\rho/\mu$
R_i	inner cylinder radius, m
R_0	outer cylinder radius, m
R^*	radial position where the angular velocity gradient is zero, m
$\hat{R}^*$	dimensionless radial position where the angular velocity gradient is zero, $\hat{R}^* = R^*/R_i$
r	radial coordinate in cylindrical coordinates, m
$\hat{r}$	dimensionless radial coordinate in cylindrical coordinates, r/R_i
v_{ave}	average angular velocity, $(R_i+R_0)\omega/2$, m/s
v_θ	velocity component in θ-direction, m/s
$\hat{v}_\theta^+$	dimensionless angular velocity with positive velocity gradient, $v_\theta^+/R_i\omega$
$\hat{v}_\theta^-$	dimensionless angular velocity with negative velocity gradient, $v_\theta^-/R_i\omega$

Greek letters

Δ	rate of deformation tensor, s^{-1}
η	apparent viscosity, Pa·s
κ	ratio of R_i and R_0
ω	angular rotation speed, rad/s
θ	angular coordinate in cylindrical coordinates
μ	Newtonian viscosity, Pa·s
ρ	density, kg/m^3
τ	shear stress, Pa
$\tau_{r\theta}$	shear stress on plane perpendicular to r in the direction of θ
$\partial P/\partial\theta$	pressure gradient in cylindrical coordinate θ-direction

REFERENCES

ABICHANDANI, H., SARMA, S.C. and HELDMAN, D.R. 1987. Hydrodynamics and heat transfer in liquid full scraped surface heat exchangers — a review. J. Food Process Engineering *9*, 121–141.

AROLA, D.F., BARRALL, G.A., POWELL, R.L., McCARTHY, K.L. and MCCARTHY, M.J. 1997. Use of magnetic resonance imaging as a viscometer for process monitoring. Chemical Engineering Sci. *52*, 2049–2057.

BIRD, R.B., STEWART, W.E., and LIGHTFOOT, E.N. 1960. *Transport Phenomena*, John Wiley & Sons, New York.

CAPRIHAN, A. and FUKUSHIMA, E. 1990. Flow measurement by NMR. Physics Reports *198*, 195-235.

CORBETT, A.M., PHILLIPS, R.J., KAUTEN, R.J. and McCARTHY, K.L. 1995. Magnetic resonance imaging of concentration and velocity profiles of pure fluids and solid suspensions in rotating geometries. J. Rheol. *39*, 907-924.

CRC, 1991. *CRC Standard Mathematical Tables and Formulae, 29th Edition*, (W.H. Beyer, ed.) pp. 217-224, CRC Press, Boca Raton.

HÄRRÖD, M. 1986. Scraped surface heat exchangers — A literature survey of flow patterns, mixing effects, residence time distribution, heat transfer and power requirements. J. Food Process Engineering *9*, 1-62.

MCCARTHY, M.J. 1994. *Magnetic Resonance Imaging in Foods*. Chapman & Hall, New York.

REDDY, J.N. 1984. *An Introduction to the Finite Element Method*, pp. 1-10, McGraw-Hill Book Co., New York.

SEGERLIND, L.J. 1984. *Applied Finite Element Analysis*, pp. 2-15, John Wiley & Sons, New York.

TROMMELEN, A.M. and BEEK, W.J. 1971. Flow phenomena in a scraped-surface heat exchanger ("Votator"-type). Chemical Engineering Sci. *26*, 1933-1942.

WANG, W. 1997. Experimental aspects of mixing in scraped surface heat exchanger geometry. Ph. D. thesis, University of California, Davis, CA.